Desalination and Water Treatment
www.deswater.com

doi: 10.5004/dwt.2017.21706

98 (2017) 115–122
December

A comparison between alkaline earth metal titanates for application as photocatalysts in wastewater treatment

Ionela Carazeanu Popovici[a], Georgeta Stroie[a], Georgeta Voicu[b], Florin Moscalu[c], Aurel Diacon[d], Anca Dumbrava[a,*]

[a]*Ovidius University of Constanta, Department of Chemistry and Chemical Engineering, 124 Mamaia Blvd., Constanta 900527, Romania, email: adumbrava@univ-ovidius.ro*
[b]*University Politehnica of Bucharest, Department of Science and Engineering of Oxide Materials and Nanomaterials, 1-7 Polizu Street, Bucharest 011061, Romania*
[c]*Ovidius University of Constanta, Department of Physics, 124 Mamaia Blvd., Constanta 900527, Romania*
[d]*University Politehnica of Bucharest, Department of Bioresources and Polymer Science, 1-7 Polizu Street, Bucharest 011061, Romania*

Received 12 July 2017; Accepted 19 November 2017

ABSTRACT

The alkaline earth metal titanates are ternary oxides with remarkable properties and applications. We studied the optical and photocatalytic properties of three alkaline earth metal (Ca, Sr, Ba) titanates obtained by sol-gel method, in order to be used in the treatment of wastewaters. The optical properties of titanates were determined by UV-visible and photoluminescence spectroscopy. The band gap energies were calculated using Tauc equation. The morphology of powders was evidenced by scanning electron microscopy. The photocatalytic properties were tested in the bleaching of Congo red solutions. The titanates have a satisfactory photocatalytic activity towards the azo dye, the most efficient photocatalyst being $BaTiO_3$ (a photocatalytic activity of 49.11%, after 120 min).

Keywords: Alkaline earth metal; Titanates; Band gap energy; Congo red photodegradation; Photocatalytic properties

1. Introduction

The titanates of alkaline earth metals, with perovskite structure, are interesting compounds, in particular with regard to their optical and electrical properties [1], therefore being justified the revived interest in their study. Titanates are piezoelectric or ferroelectric materials widely used in microwave devices and modern microelectronics, such as multilayer ceramic capacitors, random access memories, radar, communication systems, pressure transducers, sound detectors, etc. [2,3]. Because of their high chemical, structural, and thermal stability, the alkaline earth metal titanates are also used in various photocatalysis applications, like the water splitting (*e.g.* Sb and Rh doped $SrTiO_3$ [4], $SrTiO_3$ in presence of a NiO co-catalyst [5]), photodegradation of organic dyes like methylene blue (*e.g.* nanopowders of $CaTiO_3$, $SrTiO_3$ and $BaTiO_3$ [6]) or other dyes [7–9]. Biocompatibility studies of barium titanate particles on stem cells demonstrated the possibility of application as nanovectors and enhancement of osteogenic potential of mesenchymal stem cells for bone regeneration or, because of non-linear optical properties of $BaTiO_3$, the nanoparticles can be used in fluorescent probes for biological applications and multiphoton microscopy [10]. The synthesis of calcium, strontium and barium titanates by sol-gel method was extensively reported by Pfaff [1,11,12], but it was also described in other studies [*e.g.* 13]. The physical and chemical properties of titanates are strongly related with their size, shape, and surface chemistry [2].

The various properties of perovskite oxides (ABO_3), including the alkaline earth metal titanates, could be traced to their crystal and electronic structures. An ideal perovskite has a cubic crystal structure, which is composed of a three dimensional framework of BO_6 octahedrons

*Corresponding author.

connected via their vertices, the BO_6 octahedron being considered the basic cell. The A-site cation is often alkaline earth metal or rare earth element, while B-site cation is often transition metal; B site cation locates in octahedral vacancy and A site cation fills the 12-coordinate cavities formed by BO_6 network [14]. A rigorous understanding of the structure *vs.* property relations involves extensive electronic structure calculations [15], based on density functional theory, but a qualitative understanding is possible on the basis of chemical bonding considerations [16]. In the ideal perovskite structure with a cubic symmetry, the atoms are connected to one another and a relationship was established between the ionic radii. Thus, for perovskite oxides can be considered the relation:

$$r_A + r_O = \sqrt{2}\left(r_B + r_O\right) \quad (1)$$

where r_A, r_B and are the ionic radii of A, B and O-site elements, respectively. The relative ionic size requirements for stabilizing the cubic structure are quite stringent. Therefore, slight buckling and distortion can produce several lower-symmetry distorted versions, in which the coordination numbers of the A cations, B cations or both are reduced. The tolerance factor (t), first introduced by Goldschmidt, can evaluate the deviation from the ideal structure, being defined by the following equation [17]:

$$t = \frac{r_A + r_O}{\sqrt{2}(r_B + r_O)} \quad (2)$$

It has been generally accepted that perovskites can be stabilized when t ranges between 0.76 and 1.13, but t = 1 for the ideal cubic perovskite [18]. If t shows deviation from 1, it might indicate the formation of a perovskite structure of non-ideal type [17]. Afterwards, the octahedral factor (μ, $\mu = \frac{r_B}{r_O}$ for oxides) was also proposed for assessing the stability of a perovskite structure [18,19].

The purpose of our study was to emphasize the relevance of alkaline earth metal for the properties of titanates, A^ETiO_3 (A^E = Ca, Sr, Ba), and their application as photocatalysts. We studied $CaTiO_3$ [20], $SrTiO_3$ [21] and $BaTiO_3$ [22] synthesized by a sol-gel method, in similar experimental conditions. The considered titanates were previously characterized by X-ray diffraction (XRD) and transmission electron microscopy (TEM) [20–22]. The optical and electrical properties, and also the photocatalytic activity of A^ETiO_3 powders were comparatively discussed, taking into account the influence of alkaline earth metal and the morphological characteristics.

2. Experimental

2.1. Materials and synthesis

The high purity reagents were obtained from Sigma-Aldrich (titanium(IV) butoxide, $Ti(OC_4H_9)_4$; strontium nitrate, $Sr(NO_3)_2$; barium nitrate, $Ba(NO_3)_2$; ethylene glycol, $HOCH_2CH_2OH$; ethylenediaminetetraacetic acid, H_4EDTA; nitric acid 63%, HNO_3; Congo red) and Merck (calcium acetate, $Ca(CH_3COO)_2{\cdot}xH_2O$; ammonia solution, NH_3 25%; titanium dioxide, TiO_2), being used as received without further purification. The synthesis of $CaTiO_3$ [20], $SrTiO_3$ [21] and $BaTiO_3$ [22] was carried out as it was previously reported.

2.2. Properties of A^ETiO_3 powders

The scanning electron microscopy was performed on a Hitachi S 2600 N microscope, using an electron beam accelerated at 500 V to 30 kV. The UV-visible diffuse reflectance spectra of A^ETiO_3 powders were recorded in the range of 220–850 nm, on a Jasco V 550 spectrophotometer with an integrating sphere, using MgO as the reference. The photoluminescence spectra were recorded on a Jasco FP-6500 spectrofluorometer.

The photocatalytic properties of A^ETiO_3 samples were tested in the degradation of Congo red azo dye, using 100 mL of 30 mg/L CR solution and 0.05 g of A^ETiO_3 as catalyst. For comparison, the same experiments were also performed using a commercially available TiO_2 powder. Congo red (CR, C.I. Direct Red 28, M.W. = 696.67 g mol^{-1}, $C_{32}H_{24}N_6O_6S_2Na_2$) is the disodium salt of 3, 3'-([1,1'-biphenyl]-4,4'-diyl)bis(4-aminonaphthalene-1-sulfonic acid). The experiments were performed in the same time with two samples, in laboratory ambient light and also using an additional 45 W halogen lamp, which matches with the solar spectrum, as simulated solar light source (denoted as "light"). For the photocatalytic experiments, we followed the previously published procedure [23]. The CR degradation was monitored by UV-vis spectroscopy. The UV-vis absorption spectra of CR solutions were recorded in the range of 200–900 nm, on a Jasco V 550 spectrophotometer. The absorption peaks corresponding to CR appeared at 497 nm, 347 nm and 237 nm [23].

The dye degradation was estimated by C_t/C_0 ratio, where C_t and C_0 are the concentration of CR at certain time, t, and initial concentration, respectively. The catalyst efficiency was determined by the photocatalytic activity (*PA*) [23,24]:

$$PA = \frac{C_0 - C_t}{C_0} \cdot 100 = \frac{A_0 - A_t}{A_0} \cdot 100 \quad (3)$$

where A_0, A_t are the absorbance value for CR solutions when the reaction time is 0 and t, respectively, as it results from Lambert–Beer law.

3. Results and discussion

The deviations from the ideal structure, calculated on the basis of the Goldschmidt equation [17] and using the ionic radii values (N.C. = 6) for Ti^{4+} (61 pm), Ca^{2+} (100 pm), Sr^{2+} (126 pm), Ba^{2+} (142 pm), O^{2-} (140 pm) [25], are: t_{CaTiO_3} = 0.8443; t_{SrTiO_3} = 0.9358; t_{BaTiO_3} = 0.9921; all three values are in the rage of perovskite stability [18]. The structure closest to ideal cubic perovskite is expected for $BaTiO_3$.

3.1. Morphology of A^ETiO_3 powders

The morphology of A^ETiO_3 powders (Fig. 1) was studied by scanning electron microscopy (SEM).

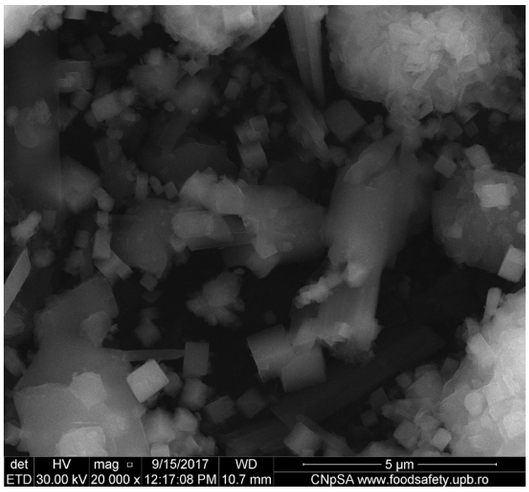

(a)

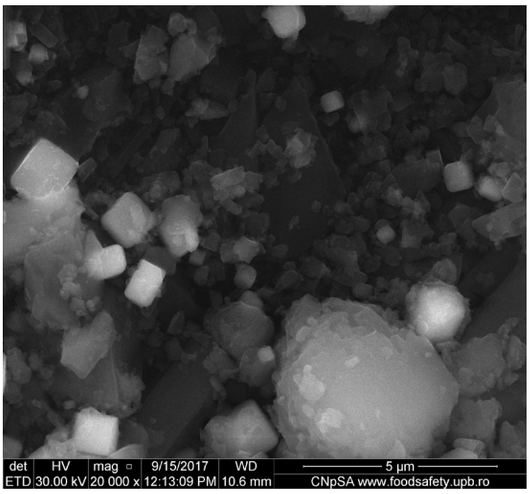

(b)

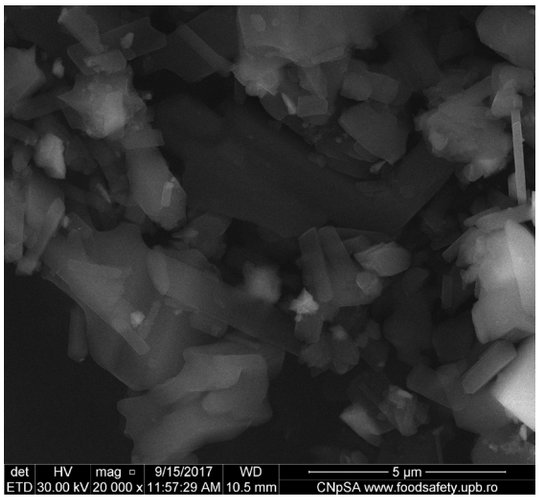

(c)

Fig. 1. The SEM images of $CaTiO_3$ (a), $SrTiO_3$ (b) and $BaTiO_3$ (c) powders.

The alkaline earth metal titanates are bulk materials, with particles dimension over 100 nm. Mixtures of cubic and rectangular particles were identified for all samples. Previous studies [26] evidenced three types of shape for $CaTiO_3$ particles and demonstrated that rectangular particles have a higher photocatalytic activity, superior to that of cubic and spherical particles.

3.2. UV-Vis spectroscopy

The optical properties of the synthesized A^ETiO_3 powders were studied by the UV-visible diffuse reflectance and photoluminescence spectroscopy. The UV-vis absorption spectra are shown in Fig. 2; for comparison, the spectrum of a commercial TiO_2 powder (Merck) was also registered.

The optical properties of perovskites, such as reflectivity or absorption, can be related with the electronic structure of the solid through the optical dielectric function. The electric conduction is three-dimensional along the TiO_6 network, which is stable for substitution with alkaline earth metals [17]. Many of the titanates properties can be understood in terms of the electronic structure of the TiO_6 octahedron in its undistorted form, which is also found in TiO_2. The distortion of TiO_6 octahedron, which modifies the symmetry, the fundamental and excites sites, the electronic transitions, and therefore the electronic spectra of titanates, can be due to the volume and the electronegativity of A^E(II) ions. However, the A^E site cations in A^ETiO_3 are in general strongly electropositive and hence they play a secondary role in the electronic structure. Their size plays often a crucial role in modifying the TiO_6 connectivity of the titanate structure and consequently the electronic structure [16].

The spectra of A^ETiO_3 (A^E = Ca, Sr, Ba) are similar to the TiO_2 spectrum in the UV domain (Fig. 2). The difference consists in the position of bands, which can be correlated with the band gap energy and particles dimension. Thus, the TiO_2 spectrum most intense band, at 324 nm, is slightly shifted to 322 nm ($CaTiO_3$), 343 nm ($SrTiO_3$), respective 326 nm ($BaTiO_3$).

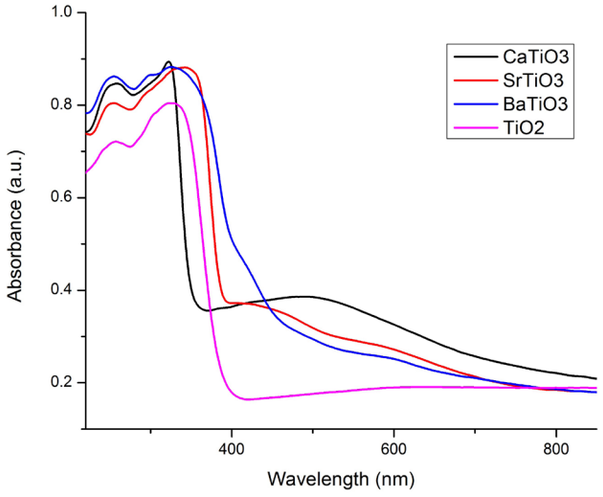

Fig. 2. The UV–vis absorption spectra of A^ETiO_3 powders, in comparison with TiO_2.

The electronic spectra of A^ETiO_3 differ more in the visible domain. In the $CaTiO_3$ spectrum, the supplementary band (compared to TiO_2 spectrum) is situated at highest wavelength (491 nm), so at lowest energy, meaning the lowest energy difference between the new energy levels, occurring due to the A^E(II) ions. As the alkaline earth metal volume and the electropositive character increased, the absorption bands are moved to lower wavelength (403 nm for $SrTiO_3$ and overlapping for $BaTiO_3$) thus higher energies; for $BaTiO_3$ the band is shifted in the UV domain, with consequences regarding the powder color. Furthermore, a supplementary band, and thus a supplementary distortion and splitting, can be observed in $BaTiO_3$ spectrum.

3.3. Band gap energy

The initiation of a photocatalytic reaction requires a minimum photon energy that exceeds the band gap of the catalyst, therefore reducing the band gap of TiO_2 and titanates can enhance the photocatalytic performance through more efficient utilization of lower energy photons [27]. The importance of band gap energy and the tuning of its value by the synthesis method was revealed, for example, in application of alkaline earth metal titanates for solar hydrolysis-splitting water into hydrogen and oxygen molecules using visible light [28]. Due to the large difference in electronegativity between oxygen and titanium atoms (3.44 *vs.* 1.54 for Pauling electronegativity) the optical band gaps for TiO_2 are slightly above 3 eV (rutile 3.0 eV, anatase 3.4 eV, and brookite 3.3 eV) [29]. For the same reason, some perovskite oxides, such as alkaline earth metal titanates, have also wide band gaps (3–5 eV) [30]. The values for Pauling electronegativity (χ_P) of alkaline earth metals are as follows: Ca - χ_P = 1.00; Sr - χ_P = 0.95; Ba - χ_P = 0.89 [31]. Significant lower band gaps (1.45–2.15 eV) were determined from UV-vis diffuse reflectance measurements for other perovskites [18].

Some authors communicated that $SrTiO_3$ in its stoichiometric form (Sr:Ti:O = 1:1:3) has a 3.2 eV band gap (at T = 0 K). However, the presence of intrinsic defects, such as vacancies, and the appearance of extrinsic defects like dopants lead to modifications of the electronic structure and the electronic conductivity of the material. The *p*-type conductivity may arise from the incorporation of oxygen into the impurity induced oxygen vacancies [16]. The band gap for the $SrTiO_3$ film fired at 600°C, obtained by an alternative method using EDTA, was around 3.4 eV, close to the reported single crystal value [32].

The band gap energy (E_g) of A^ETiO_3 powders was estimated from the UV-vis reflectance spectra using the Tauc relation [33]. The Tauc plot (Fig. 3) can be drawn of $(\alpha h\nu)^2$ versus $h\nu$, where α is the absorption coefficient of the A^ETiO_3 at a certain value of wavelength λ, h is Planck's constant, C is the proportionality constant, ν is the frequency of light. The point of the extrapolation of the linear part that meets the abscissa will give the value of the band gap energy of the material [33].

The E_g values increase from $BaTiO_3$ to $CaTiO_3$, with the decrease of the ionic radius and the increase of the electronegativity. The E_g values for $CaTiO_3$ and $BaTiO_3$ are higher to those of TiO_2. The E_g value for $SrTiO_3$ is expected to be between those for $CaTiO_3$ and $BaTiO_3$, so the calculated value can be due to the lattice defects or nonstoichiometry

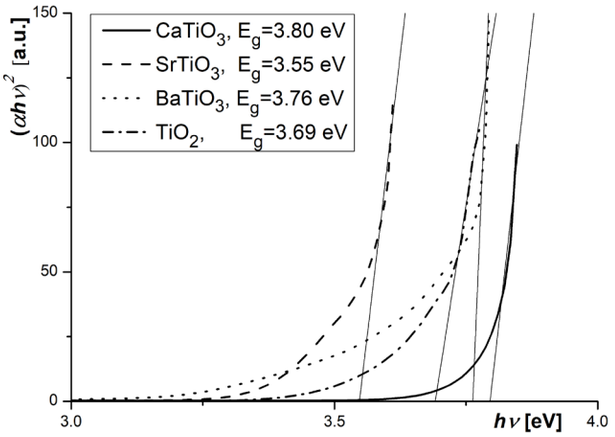

Fig. 3. Tauc plots for A^ETiO_3 samples, in comparison with TiO_2.

of $SrTiO_3$. The defect chemistry responsible for accommodating either excess A^EO or excess TiO_2 is currently unclear [34]. It is know that the variation of the A-site cation in titanates can affect the optical properties by deforming the TiO_6 octahedron network. A larger or smaller A^E cation can cause the entire lattice to expand or contract and lead to a change in the Ti–O bond length, which has been reported to be important for determining the band gaps [18]. Because the electronegativity of alkaline earth metal influences the energy levels in the titanate, and thus the band gap energy, the highest electronegativity for Ca can explain the highest energy band for studied alkaline earth titanates.

3.4. Photocatalytic properties

The treatment of wastewaters contaminated with toxic organic compounds is an issue of high interest for scientists, the use of semiconductor catalysts being a promising method for the organic pollutants destruction [14]. Among the semiconductors, TiO_2 has been considered one of the most desirable photocatalysts [14,35]. Despite numerous advantages of TiO_2 material (like long-term stability, nontoxic environmental acceptability and broadly low cost availability), it is photoactive only in the UV region of the electromagnetic spectrum. The materials which combine the advantages of TiO_2 with an absorption in visible domain, such as titanates, can be sustainable alternatives for TiO_2 photocatalysts.

The perovskite-type oxide materials have achieved significant attention in pollution reduction and environmental remediation. One advantage of perovskite type structure is the valence and vacancy control, which enhances their catalytic activity. The mechanism of ABO_3 perovskite type oxides in catalytic reactions can be explained by two main features: (*i*) the corner shared BO_6 octahedron network can facilitate electron and oxygen transfer, ultimately leading to oxygen non stoichiometry, making perovskites excellent catalysts for the degradation of pollutant by inducing high reducibility; (*ii*) the atoms at A-site of ABO_3 help the stabilization of multiple valence states of B site cation, which will make the electrons of ABO_3 oxides more active and be excited easily

by the external energy such as light irradiation and transfer [9,36]. It was reported that in some perovskites, because of their narrower depletion layers, separation of electrons and holes is easier in comparison to TiO_2 [37]. In brief, the mechanism of azo dyes degradation through photocatalytic processes, as it was described for $BaTiO_3$ [38], involves in the photoexcitation of particles under the illumination, promoting charge separation with generation of electrons. The generated electron is promoted from the valence band to conduction band and the conduction band electron can migrate to the surface of titanate. Consequently, the oxygen adsorbed on the surface is able to react with the photoelectron and a series of strong oxidative free radicals is synthesized. The positive charged hole formed in the valence band can react with H_2O to generate ·OH radical. The radicals further react with azo dye, producing a whole range of intermediates till the complete mineralization with the synthesis of carbon dioxide, water, nitrogen, and anions like nitrate, ammonium, sulfate and chloride.

The catalytic properties of obtained A^ETiO_3 powders were demonstrated in the photocatalytic degradation of Congo red solutions. The concentration of CR is estimated from the intensity of the absorbance band at λ = 497 nm, characteristic to azo bond. The decrease of absorbance band intensity in UV-visible spectra indicates the disappearance of CR by breaking up the azo bond (the azo bond degradation) as a function of irradiation time. The bleaching of the solutions was estimated by the C_t/C_0 ratio (Fig. 4), using the CR concentrations calculated from the absorbance values of the CR solutions.

The catalytic activity is quite similar for the A^ETiO_3 powders, with minor differences and a small increase with the illumination of samples. Thus, after 120 min, PA is: 38.60% ($CaTiO_3$), 44.18% ($CaTiO_3$, light), 33.41% ($SrTiO_3$), 40.57% ($SrTiO_3$, light), 41.56% ($BaTiO_3$), 49.11% ($BaTiO_3$, light). The photocatalytic activity of titanates was comparable (for $BaTiO_3$) or inferior (for $CaTiO_3$ and $SrTiO_3$) to that of TiO_2 powder, in similar photocatalytic conditions. The bleaching of azo dye solution in absence of catalyst is insignificant, namely around 3% after 120 min [40].

The highest photocatalytic activity (Fig. 4) was observed for $BaTiO_3$ with the band gap energy of 3.76 eV, smaller than for $CaTiO_3$. The abnormal low value of E_g for $SrTiO_3$ was not sustained by the photocatalytic activity, but the increase of photocatalytic activity from $CaTiO_3$ to $BaTiO_3$ is in concordance with their optical properties. Once again, the unexpected results for $SrTiO_3$ can be due to its structure. Most probably, a high concentration of defects in $SrTiO_3$, which was also suggested by E_g value, is a key explanation for this behavior. It was demonstrated that both intrinsic and foreign defects are important in photocatalysis. They act as trappers of electrons and holes, mainly forming the recombination centers. After the electrons and holes are photogenerated, the holes can be quickly trapped on surface defects, or transferred to organic species, so the defect distribution and concentration play an important role in the electron transport [41].

In addition to the defects, the material morphology also has an obvious effect on photocatalytic activity [41]. The SEM images evidenced the irregularity of particles shape and different ratio between cubic and rectangular particles, with different photocatalytic activities, which can explain

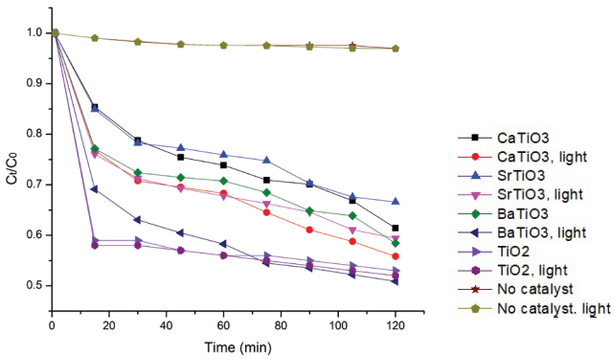

Fig. 4. The photocatalytic degradation curves of CR over catalysts (A^ETiO_3 and TiO_2) or no catalyst [39], in different conditions.

the differences in photocatalytic activity of studied powders. Another explanation involves particles dimension. The primary particle size of a material influences its photocatalytic properties, both through specific surface area and the photon conversion efficiency. During the synthesis, the particles are agglomerated and the secondary particles size also influences the photocatalytic process [26]. By TEM investigation, the secondary particle size (for aggregates) were determined as mean diameter of measured particles [42]. The evaluation of mean diameter was performed using a semi-automated algorithm implemented in the analysis software. The values were 121.98 nm ($CaTiO_3$) [20], 198.12 nm ($SrTiO_3$) [21] and 105.45 nm ($BaTiO_3$) [22]. The lower dimension for $BaTiO_3$ aggregates, meaning a higher specific surface area, can be another explanation for its best photocatalytic activity. The obviously higher mean diameter for $SrTiO_3$ aggregates can be correlated with a lower surface area and a lower capacity for adsorption, which justify the lowest photocatalytic activity. The photocatalytic activity is also influenced by the solution pH. A suspension of A^ETiO_3 powder in water involves a high value of pH, which is not favorable for photocatalytic process [39], but the pH value was similar for studied titanates (pH ≈ 10). The photocatalytic activity determined for A^ETiO_3 was inferior to other titanates (*e.g.* quaternary oxides like $La_{0.8}Ba_{0.2}TiO_{3.5-\delta}$[9]), this property being related with many factors, including the nature and properties of A site metal.

Congo red, a benzidine-based anionic disazo dye, is toxic to many organisms and suspected carcinogen and mutagen, being highly resistant to the biodegradation and its removal from wastewaters is an important environmental problem [43]. Benzidine can be one of the CR degradation products, so the simple breakdown of the azo bonds (the chromophores) is not enough for the environmental safety [44]. As one can see in Fig. 5, the UV-vis spectra demonstrated that the CR solution is not only bleached, but the dye is decomposed, the intensity of band assigned to aromatic rings in the electronic spectra decreasing also in time. The ratio between the intensity of the bands assigned to azo group, respective to aromatic rings decreased in time, proving a faster breakdown of azo bond in comparison with the degradation of aromatic rings. In a detailed study, the phenol was identified as one of aromatic intermediates from photocatalytic degradation of CR over TiO_2 catalyst [45].

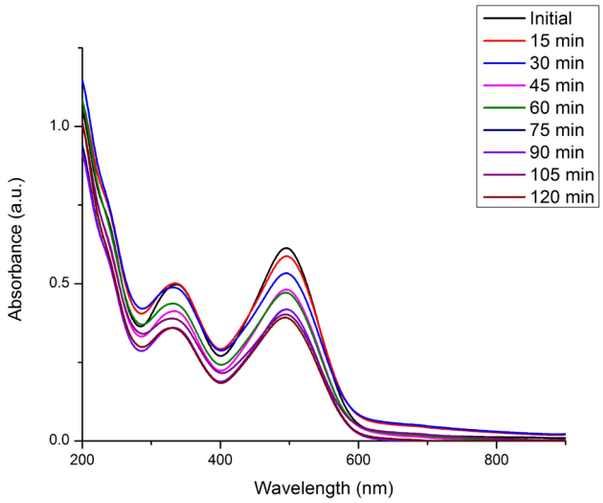

Fig. 5. The UV-vis spectral changes of RC solution during the photodegradation over $BaTiO_3$ catalyst, as function of time (with supplementary illumination).

3.5. Photoluminescence spectroscopy

The photoluminescent properties of alkaline earth metal titanates were investigated by the photoluminescence (PL) spectroscopy, under excitation with different wavelengths (Fig. 6). Usually, two emissions (excitonic and trapped photoluminescence) are observed in PL spectra of semiconductors; the excitonic emission is sharp and found near the absorption edge, while the trapped emission is broad and found at higher wavelength [46].

The emission bands at 467 nm (Fig. 5a,b), with the same wavelength for all titanates, have different intensities. The values of intensity increase from $CaTiO_3$ to $SrTiO_3$ and $BaTiO_3$, with a regular variation. For bands around 286 nm and 420 nm (Fig. 5a) similar positions were also observed, but the variation of intensity is irregular, increasing from $SrTiO_3$ to $CaTiO_3$ and $BaTiO_3$, respective from $CaTiO_3$ to $BaTiO_3$ and $SrTiO_3$. The dissimilarity of PL spectra for studied titanates is most visible for the excitation with a laser irradiation at wavelength of λ = 340 nm. The position of emission maxima in 350–400 nm domain is different for $SrTiO_3$ spectrum in comparison with $CaTiO_3$ and $BaTiO_3$ spectra. An explanation for these differences involves the existence of defects in $SrTiO_3$.

The relationship between photoluminescent and photocatalytic properties is complex and must have in view different types of recombination, which can occur in titanates. It was demonstrated [47,48] that electrons and holes are generated under the photoexcitation and the photoexcited electrons transit to the conduction band and fill the energy levels, which correspond to excitation energy. These electrons and holes can easily recombine and return to valence band in different ways, and their energy can be emitted as photons or phonons. Two types of radiative transitions can take place: (*i*) direct radiative transitions, when excited electrons can transit directly to valence band with release of energy in the form of light emission, in case of electrons with higher energy than E_g and (*ii*) indirect radiative transition, when the recombination process occurs

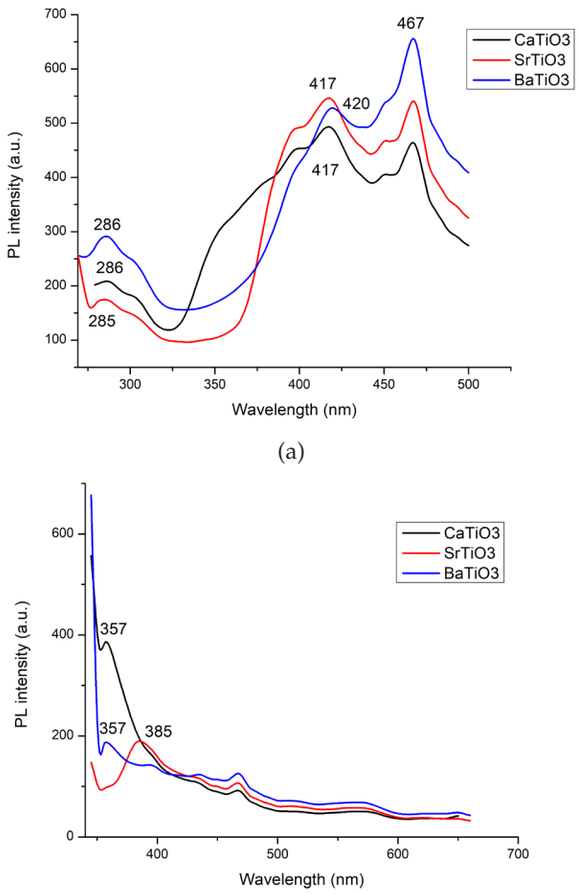

Fig. 6. PL emission spectra of A^ETiO_3 powders under 265 nm (a) and 340 nm (b) excitation.

through sublevels in energy band gap (*e.g.* defect states of the matrix). In some cases, lower recombination causes smaller photoluminescence intensity and higher photocatalytic activity of semiconductor, but in other cases the increase of defects amount and oxygen vacancies at the surface allows to obtain higher intensity of photoluminescence and photocatalytic activity [47–49]. So, most often it is necessary to elaborate an individual model, taking into consideration properties of materials and mechanisms occurring during both direct and indirect radiative transitions.

3.6. Kinetic study

A detailed analysis of photocatalytic kinetics is complicated because of many processes involved in such heterogeneous systems, but many experimental results demonstrated that the decomposition rates in azo dyes photocatalytic oxidation over TiO_2 fitted the widely accepted and used Langmuir–Hinshelwood (L–H) kinetic model [41,50].

The L-H simplified equation [50,51] can be written in a linearized form:

$$\ln C_t = \ln C_0 - k_{app} \cdot t \quad (4)$$

Table 1
Kinetic parameters for photocatalytic degradation of CR over A^ETiO_3

Kinetic parameters	Photocatalyst					
	$CaTiO_3$	$CaTiO_3$, light	$SrTiO_3$	$SrTiO_3$, light	$BaTiO_3$	$BaTiO_3$, light
k_{app} (min^{-1})	$2.7 \cdot 10^{-3}$	$2.9 \cdot 10^{-3}$	$2.2 \cdot 10^{-3}$	$2.2 \cdot 10^{-3}$	$2.3 \cdot 10^{-3}$	$2.8 \cdot 10^{-3}$
R^2	0.958	0.980	0.954	0.977	0.941	0.954

where C_t is the concentration of CR (mg/L), C_0 - the initial value of concentration, t – the illumination time, and k_{app} is the pseudo fist order rate constant (min^{-1}). The values of correlation coefficients (R^2) for the linear plots of ln C_t versus irradiation time confirm a L-H kinetic type. The pseudo fist order rate constant (k_{app}) for the photocatalytic degradation of CR was also evaluated from experimental data, using a linear regression (Table 1).

Similar rate constant values were calculated for all titanates. For $CaTiO_3$ and $BaTiO_3$ a supplementary illumination slightly increased the reaction rate. In concordance with other experimental data presented above, the lowest values for rate constant were assigned to $SrTiO_3$. The lower values of rate constant for $BaTiO_3$ compared to $CaTiO_3$, in spite of a superior photocatalytic activity, can be correlated with a higher adsorption capacity.

4. Conclusions

We tested the photocatalytic properties of alkaline earth metal titanates in the bleaching of CR solutions, with applications in the treatment of wastewaters for textile industry. All three titanates are wide-band semiconductors, with band gap energies superior (for $CaTiO_3$ and $BaTiO_3$) or inferior (for $SrTiO_3$) to that of a TiO_2 sample. The best catalytic activity was assigned to $BaTiO_3$. The photocatalytic activity can be correlated with the alkaline earth metal properties (especially with the volume and electronegativity, which influence the energy levels and consequently the bang gap energy) and with the powder morphology, respective the dimension and shape of particles and their aggregates. A good correlation can be done for $CaTiO_3$ and $BaTiO_3$. The uncharacteristic position of $SrTiO_3$ can be explained, very probably, on the basis of the lattice defects, as the PL spectra and E_g values also suggested.

References

[1] G. Pfaff, Synthesis of calcium titanate powders by the sol-gel process, Chem. Mater., 6 (1994) 58–620.
[2] Q. Ma, K. Mimura, K. Kato, Tuning shape of barium titanate nanocubes by combination of oleic acid/tert-butylamine through hydrothermal process, J. Alloy. Compd., 655 (2016) 71–78.
[3] B.A. Hernandez-Sanchez, T.J. Boyle, C.M. Baros, L.N. Brewer, T.J. Headley, D.R. Tallant, M.A. Rodriguez, B.A. Tuttle, Alkaline earth titanate (A^ETiO_3) perovskite nanoparticles synthesized from structurally characterized single-source alkoxides, Chem. Mater., 19 (2007) 1459–1471.
[4] R. Niishiro, S. Tanaka, A. Kudo, Hydrothermal-synthesized $SrTiO_3$ photocatalyst codoped with rhodium and antimony with visible-light response for sacrificial H_2 and O_2 evolution and application to overall water splitting, Appl. Catal. B Environ., 150–151 (2014) 187–196.
[5] T.K. Townsend, N.D. Browning, F.E. Osterloh, Nanoscale strontium titanate photocatalysts for overall water splitting, ACS Nano, 6 (2012) 7420–7426.
[6] T. Alammar, I. Hamm, M. Wark, A.V. Mudring, Low-temperature route to metal titanate perovskite nanoparticles for photocatalytic applications, Appl. Catal. B Environ., 178 (2015) 20–28.
[7] B. Lertpanyapornchai, T. Yokoi, C. Ngamcharussrivichai, Citric acid as complexing agent in synthesis of mesoporous strontium titanate via neutral-templated self-assembly sol-gel combustion method, Micropor. Mesopor. Mater., 226 (2016) 505–509.
[8] S. Otsuka-Yao-Matsuo, T. Omata, S. Ueno, M. Kita, Photobleaching of methylene blue aqueous solution sensitized by composite powders of titanium oxide with $SrTiO_3$, $BaTiO_3$, and $CaTiO_3$, Mater. Trans., 44 (2003) 2124–2129.
[9] M. Bradha, T. Vijayaraghavan, S.P. Suriyaraj, R. Selvakumar, A.M. Ashok, Synthesis of photocatalytic $La_{(1-x)}A_xTiO_{3.5-\delta}$ (A=Ba, Sr, Ca) nano perovskites and their application for photocatalytic oxidation of Congo red dye in aqueous solution, J. Rare Earth., 33 (2015) 160–167.
[10] L.R. Prado, N.S. de Resende, R.S. Silva, S.M.S. Egues, G.R. Salazar-Banda, Influence of the synthesis method on the preparation of barium titanate nanoparticles, Chem. Eng. Process. Proc. Intens., 103 (2016) 12–20.
[11] G. Pfaff, Sol–gel synthesis of strontium titanate powders of various compositions, J. Mater. Chem., 3 (1993) 721–724.
[12] G. Pfaff, Sol–gel synthesis of barium titanate powders of various compositions, J. Mater. Chem., 2 (1992) 591–594.
[13] C. Lemoine, B. Gilbert, B. Michaux, J.P. Pirard, A.J. Lecloux, Synthesis of barium titanate by the sol-gel process, J. Non Cryst. Solids, 175 (1994) 1–13.
[14] Y. Yang, Y. Sun, Y. Jiang, Structure and photocatalytic property of perovskite and perovskite-related compounds, Mater. Chem. Phys., 96 (2006) 234–239.
[15] K.K. Saha, T. Saha-Dasgupta, A. Mookerjee, S. Saha, T.P. Sinha, Optical properties of perovskite alkaline earth titanates: a formulation, J. Phys. Condens. Mat., 14 (2002) 3849–3863.
[16] F.M.F. de Groot, M. Grioni, J.C. Fuggle, J. Ghijsen, G.A. Sawatzky, H. Petersen, Oxygen 1s X-ray-absorption edges of transition-metal oxides, Phys. Rev. B, 40 (1989) 5715–5723.
[17] V.M. Goldschmidt, Krystallbau und chemische Zusammensetzung, Ber. Dtsch. Chem. Ges., 60 (1927) 1263–1268.
[18] W. Wang, M.O. Tadé, Z. Shao, Research progress of perovskite materials in photocatalysis- and photovoltaics-related energy conversion and environmental treatment, Chem. Soc. Rev., 44 (2015) 5371–5408.
[19] C. Li, X.G. Lu, W.Z. Ding, L.M. Feng, Y.H. Gao, Z.M. Guo, Acta Crystallogr. B Struct. Sci., 64 (2008) 702–707.
[20] V. Ciupina, I. Carazeanu, E. Chirila, G. Prodan, TEM study of $CaTiO_3$ synthesized by sol-gel method, Proceedings "SPIE", 5581, 345–349.
[21] I. Carazeanu, E. Chirila, V. Ciupina, G. Prodan, Transmission electron microscopy study of the synthesized $SrTiO_3$ by sol-gel method, Proceedings "4AACD", 176–178, 2004.
[22] I. Popovici, E. Chirila, Preparation of $BaTiO_3$ ceramic powders via sol-gel method, Ovidius University Annals of Chemistry, 15 (2004) 9–12.
[23] A. Dumbrava, G. Prodan, D. Berger, M. Bica, Properties of PEG-capped CdS nanopowders synthesized under very mild conditions, Powder Technol., 270 (2015) 197–204.

[24] N. Soltani, E. Saion, W.M.M. Yunus, M. Navasery, G. Bahmanrokh, M. Erfani, M.R. Zare, E. Gharibshahi, Photocatalytic degradation of methylene blue under visible light using PVP-capped ZnS and CdS nanoparticles, Sol. Energy, 97 (2013) 147–154.
[25] C.E. Housecroft, A.G. Sharpe, Inorganic Chemistry, Second edition, Pearson Education Limited 2005.
[26] H. Zhao, Y. Duan, X. Sun, Synthesis and characterization of $CaTiO_3$ particles with controlled shape and size, New J. Chem., 37 (2013) 986–991.
[27] H. Lin, C.P. Huang, W. Li, C. Ni, S.I. Shah, Y.H. Tseng, Size dependency of nanocrystalline TiO_2 on its optical property and photocatalytic reactivity exemplified by 2-chlorophenol, Appl. Catal. B Environ., 68 (2006) 1–11.
[28] R. Comes, P.V. Sushko, S.M. Heald, R.J. Colby, M.E. Bowden, S.A. Chambers. Band gap reduction and dopant interaction in epitaxial La, Cr, Co-doped $SrTiO_3$ thin films, Chem. Mater., 26 (2014) 7073–7082.
[29] M. Landmann, E. Rauls, W.G. Schmidt, The electronic structure and optical response of rutile, anatase and brookite TiO_2, J. Phys. Condens. Matter, 24 (2012) 195503 (6 pp). Doi:10.1088/0953-8984/24/19/195503.
[30] Y. Li, X.P. Gao, G.R. Li, G.L. Pan, T.L. Yan, H.Y. Zhu, Titanate nanofiber reactivity: Fabrication of $MTiO_3$ (M = Ca, Sr, and Ba) perovskite oxides, J. Phys. Chem. C, 113 (2009) 4386–4394.
[31] P.W. Atkins, T.L. Overton, J.P. Rourke, M.T. Weller, F.A. Armstrong, Shriver and Atkins' Inorganic Chemistry, 5th ed., Oxford University Press, 2010
[32] M. Sato, T. Tanji, H. Hara, T. Nishide, Y. Sakashita, $SrTiO_3$ film fabrication and powder synthesis from a non-polymerized precursor system of a stable Ti(IV) complex and Sr(II) salt of EDTA, J. Mater. Chem., 9 (1999) 1539–1542.
[33] J. Tauc, R. Grigorovici, A. Vancu, Optical properties and electronic structure of amorphous germanium, Phys. Status Solidi B, 15 (1966) 627–637.
[34] S.T. Murphy, N.D.M. Hine, Point defects and non-stoichiometry in Li_2TiO_3, Chem. Mater., 26 (2014) 1629–1638.
[35] A.K. Ray, A.A.C.M. Beenackers, Development of a new photocatalytic reactor for water purification, Catal. Today, 40 (1998) 73.
[36] C. Duque, A. Stashans, Oxygen-vacancy defects on $BaTiO_3$ (001) surface: a quantum chemical study, Physica B Condens. Matter, 336 (2003) 227.
[37] W.M. Hou, Y. Ku, Synthesis and characterization of $La_2Ti_2O_7$ employed for photocatalytic degradation of reactive red 22 dyestuff in aqueous solution, J. Alloys Compd., 509 (2011) 5913.
[38] W.W. Lee, W.H. Chung, W.S. Huang, W.C. Lin, W.Y. Lin, Y.R. Jiang, C.C. Chen, Photocatalytic activity and mechanism of nano-cubic barium titanate prepared by a hydrothermal method, J. Taiwan Inst. Chem. Eng., 44 (2013) 660–669.
[39] A. Dumbrava, D. Berger, G. Prodan, C. Matei, F. Moscalu, A. Diacon, The influence of Triton X-100 surfactant on the morphology and properties of zinc sulfide nanoparticles for applications in azo dyes degradation, Mater. Chem. Phys., 193 (2017) 316–328.
[40] A. Dumbrava, D. Berger, G. Prodan, F. Moscalu, A. Diacon, Facile synthesis, characterization and application of functionalized cadmium sulfide nanopowders, Mater. Chem. Phys., 173 (2016) 70–77.
[41] B. Liu, X. Zhao, C. Terashima, A. Fujishima, K. Nakata, Thermodynamic and kinetic analysis of heterogeneous photocatalysis for semiconductor systems, Phys. Chem. Chem. Phys., 16 (2014) 8751.
[42] A. Dumbrava, D. Berger, G. Prodan, F. Moscalu, A. Diacon, Considerations about the dependence of PEGylated ZnS nanoparticles properties on the synthesis method, Z. Phys. Chem., 2017, in press. Doi: 10.1515/zpch-2017-0005.
[43] S. Dafare, P.S. Deshpande, R.S. Bhavsar, Photocatalytic degradation of Congo red dye on combustion synthesized Fe_2O_3, Indian J. Chem. Technol., 20 (2013) 406–410.
[44] M. Işik, D.T. Sponza, Effect of oxygen on decolorization of azo dyes by *Escherichia coli* and *Pseudomonas* sp. and fate of aromatic amines, Process Biochem., 38 (2003) 1183–1192.
[45] K. Tanaka, K. Padermpole, T. Hisanaga, Photocatalytic degradation of commercial azo dyes, Wat. Res., 34 (2000) 327–333.
[46] S. Kakarndee, S. Juabrum, S. Nanan, Low temperature synthesis, characterization and photoluminescence study of platelike ZnS, Mater. Lett., 164 (2016) 198–201.
[47] D. Wojcieszak, D. Kaczmarek, J. Domaradzki, M. Mazur, Correlation of photocatalysis and photoluminescence effect in relation to the surface properties of TiO_2:Tb thin films, Int. J. Photoenergy, 2013 (2013) 526140 (9 pp).
[48] J. Liqiang, Q. Yichun, W. Baiqi, L. Shudan, J. Baojiang, Y. Libin, F. Wei, F. Honggang, S. Jiazhong, Review of photoluminescence performance of nano-sized semiconductor materials and its relationships with photocatalytic activity, Sol. Energy Mat. Sol. Cell., 90 (2006) 1773–1787.
[49] S. Azizian, Kinetic models of sorption: a theoretical analysis, J. Colloid Interf. Sci., 276 (2004) 47–52.
[50] I.K. Konstantinou, T.A. Albanis, TiO_2-assisted photocatalytic degradation of azo dyes in aqueous solution: kinetic and mechanistic investigations. A review, Appl. Catal. B Environ., 49 (2004) 1–14.
[51] I.K. Konstantinou, T.A. Albanis, Photocatalytic transformation of pesticides in aqueous titanium dioxide suspensions using artificial and solar light: intermediates and degradation pathways, Appl. Catal. B Environ., 42 (2003) 319–335.